Measurement of Vibrational Damping at Cryogenic Temperatures for Silicon Carbide Foam and Silicon Foam Materials

Chia-Yen Peng[1a], Marie Levine[a], Lillian Shido[a]
Marc Jacoby[b], William Goodman[b]
[a]Jet Propulsion Laboratory, 4800 Oak Grove Drive, Pasadena, California, USA
[b]Schafer Corporation, Albuquerque, New Mexico, USA

ABSTRACT

The Terrestrial Planet Finder mission requires extreme dynamic stability at cryogenic temperatures in order to carry out its objectives of searching for and observing extraterrestrial planets. As a result, the ability to meet its ambitious science goals will be significantly enhanced by increasing its vibrational damping at cryogenic temperatures. Given the low inherent structural damping at cryogenic temperatures, significant reduction in vibration amplitude could be gained with only modest increases in damping on the structure. To examine the use of vibrational damping options to improve the dynamic stability of cryogenic structures, Jet Propulsion Laboratory has conducted a series of experiments to measure the damping levels of various materials at cryogenic temperatures and to search for the materials with higher cryogenic damping. This paper summarizes our experimental observations on the material damping of silicon foam and silicon carbide foam materials at cryogenic temperatures. These foam materials have been independently developed by Schafer Corporation and have properties that enable their applications in space environments with a range of temperature from 25K to 500K. These materials have been used for mirrors, and uses for foam based structures such as optical mounts and benches are currently in development. As observed from the measured damping, these two foam materials have higher damping than aluminum at cryogenic temperatures, and the damping level is relatively insensitive to temperature change from room to cryogenic temperatures. As a result, these materials may be potential candidates to achieve increased levels of cryogenic damping for the Terrestrial Planet Finder mission.

1. INTRODUCTION

The Terrestrial Planet Finder (TPF) mission is a key element of NASA's Office of Space Science (OSS) Navigator Program and is part of the roadmap for the OSS Astronomical Search for Origins (ASO) science theme. TPF's science objective is to implement NASA's new Vision: "conduct telescope searches for Earth-like planets and habitable environments around other stars" [1]. Specifically, the defining science goal for TPF is to detect radiation from Earth-like planets located in the habitable zones of solar-type stars in order to understand the formation and evolution of planets and, ultimately, of life beyond our Solar System. A detailed description of the mission and the multiple prong approach for achieving the aggressive goals has been presented in previous SPIE conference [2].

As illustrated by artist's impression in Figure 1, the TPF consists of two complementary space observatories: a mid-infrared formation-flying interferometer (TPF-I) and a visible-light coronagraph (TPF-C). TPF-I is currently in Pre-Phase A (the Advanced Study Phase) of its development. It is expected to enter into Phase A in 2010 and be launched sometime before 2020. TPF-C is being developed concurrently with the TPF-I, whose launch is anticipated in 2016. The combination of these two missions, observing over a wide wavelength range, will provide definitive characterization of extra-solar planets and planetary systems, and yield a reliable and robust assessment of habitability and the presence of signatures of life. The major scientific objectives of TPF are:

- Search for and detect any Earth-like planets in the habitable zone around nearby stars;
- Characterize Earth-like planets and their atmospheres, assess habitability and search for signatures of life;
- Carry out a program of comparative study of the constituents of planetary systems; and
- Enable a broad program of general astrophysics.

[1] Chia-Yen.P.Peng@jpl.nasa.gov; phone 818-354-1285

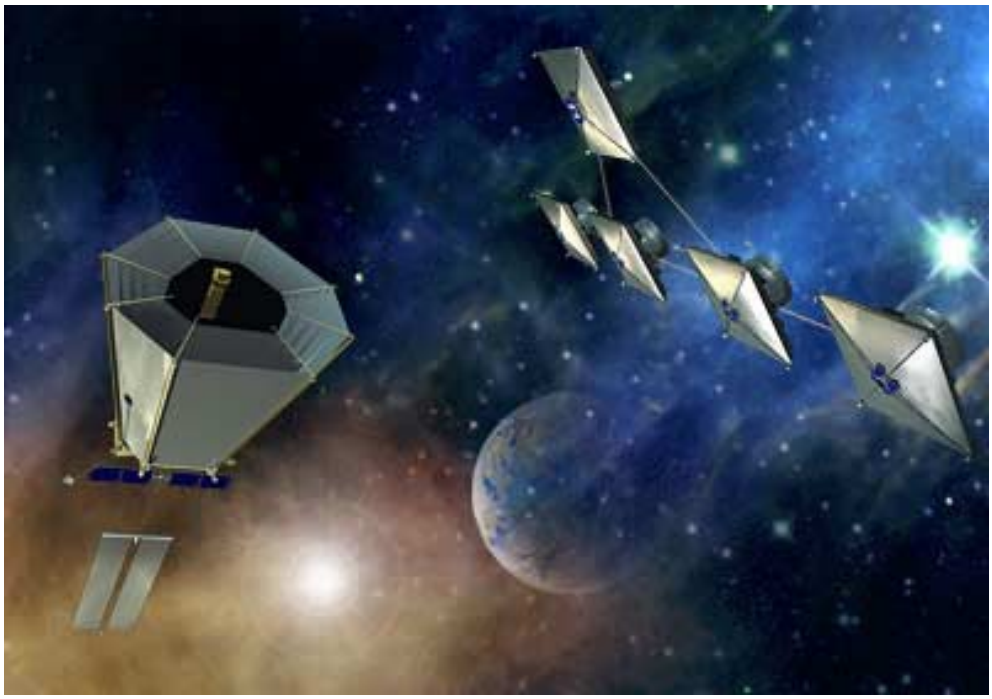

Figure 1. Artist's impression of the TPF- I (right) and the TPF-C (left).

Both TPF observatories are technologically demanding. The size of the observatories, their complexity, system tolerances, and sensitivity to environmental conditions are such that it may never be possible to undertake a full end-to-end test of the observatories prior to launch. For example, operation in the mid-infrared band dictates the need for cooling of the TPF-I optics. In order to preserve its optical performance, the current requirement is for cooling to the cryogenic temperature around 40 K. Although a detailed error budget for structural and thermal stability has not yet been flowed down to engineering design metrics, current allocations for phase control and stability suggest that the mechanical systems will need to control end-to-end optical path differences and wavefront errors down to nm levels of stability over periods of observations exceeding several hours. This implies that the TPF-I needs to maintain extreme structural and thermal stability to achieve its performance goals, which at cryogenic temperatures poses even greater technological challenges for achieving the required optical performance. In comparison, the James Webb Space Telescope (JWST) has optical path differences and wavefront error allocations are in the hundreds of nm, making the TPF-I optical performance goals approximately two orders of magnitude more challenging. Of particular concern is the technology development required for design, modeling, test validation and performance prediction of lightweight, stable, precision-composite structures for cryogenic applications.

As described above, the TPF-I telescope system needs to be maintained at cryogenic temperatures in order to reduce the thermal emissions of telescope's mirrors and their supporting structures. This is essential to achieving the required signal-to-noise ratios for the observations. In addition, very low levels of structural vibration are also required to meet the extreme structural stability requirement. Associated with small strains and extremely cold temperatures is the expected diminution of structural damping. Low structural damping degrades the quality of the optical alignment by increasing the amplitude of vibration response to on-board dynamic disturbances and by increasing the settling jitter time after spacecraft slews and maneuvers. As a result, TPF-I's ability to meet its ambitious science goals will be significantly enhanced by increasing its vibrational damping at cryogenic temperatures. Given the low inherent structural damping at cryogenic temperatures, significant reduction in vibration amplitude could be gained with only modest increases in damping on the structure. To examine the use of vibrational damping options to improve the dynamic stability of TPF-like cryogenic structures, JPL has conducted an intensive experimental effort with the following objectives:

- Provide an insight into the material damping levels at cryogenic temperatures to enable accurate system level models for prediction and control of instrument disturbances;
- Search for materials with high cryogenic damping to improve the dynamic stability of cryogenic structures.

Note that the most basic vibration damping of any built-up structure derives from the contribution of structural material itself as opposed to the usual structural damping from structural joints. However, material damping is a function not only of material, but also of the following factors:

- Temperature
- Frequency
- Geometry
- Configuration
- Strain sense and amplitude
- Environmental effects

In the case of laminated composite materials, fiber volume ratio, lay-up orientation, and internal damage from past loading events also play a significant role. This complicates the comparison between different tests and makes it difficult to extrapolate test results to other situations that are under the conditions different from the test.

This paper summarizes an on-going experimental effort to search for the materials with higher cryogenic damping. In particular, we will report our experimental observations on the material damping of silicon foam and silicon carbide foam materials at cryogenic temperatures. In general, the testing described herein is unique and has not been reported or performed previously - to the best of authors' knowledge.

2. SILICON FOAM AND SILICON CARBIDE FOAM

The silicon foam and silicon carbide foam specimens used to measure the material damping at cryogenic temperatures were provided by Schafer Corporation, a qualified Small Business, using two novel lightweight foam core mirror technologies - Silicon Lightweight Mirror Systems (SLMS™) and Silicon Carbide- Lightweight Mirror Systems (SiC-SLMS™). Both materials are quickly and inexpensively super-polishable (figure of $\lambda/10$ P-V @ 633 nm, 10 Å rms surface finish readily achieved), stiff (high and tunable first fundamental frequency), lightweight (area density as low as 5 kg/m^2), and have superior thermal properties over a broad range of temperatures, and do not out-gas. This unique combination of properties makes both materials attractive as a replacement for beryllium, Zerodur and Ultralow Expansion (ULE) glass mirrors. Both SLMS™ and SiC-SLMS™ are able to simultaneously match the weight and stiffness of beryllium mirrors while providing the equivalent transient distortion of Zerodur or ULE.

SLMS™ and SiC-SLMS™ mirror technologies have been developed and demonstrated under funding from NASA, Air Force Research Laboratory, Air Force, Missile Defense Agency and Army Space and Missile Defense Command funding. Key demonstrations have been made possible by Schafer Internal Research and Development funding. The ceramic foam core materials, in conjunction with Schafer's composite design experience, makes possible the engineered properties and performance of these unique mirror technologies. It is also in the process of designing lightweight, dimensionally stable optical mounts, optical benches, and optical structures using these novel ceramic foam materials. These materials are an enabling technology for both cryogenic and high-energy laser applications.

Figures 2-3 show that the microstrain versus temperature for Schafer's silicon and silicon carbide foam materials has little slope change from 100 K to 300 K, and is almost constant below ~100 K, meaning that the derivative or instantaneous CTE below 100 K for these materials is zero. Figure 4 confirms that the CTE of silicon foam and bulk silicon material is identical, an expected result from solid state theory. The minor differences at the extremes of the curves are attributed to a higher experimental uncertainty in the 1997 Lyons data. The 2005 Schafer's CTE data have been certified by PMIC to 0.01 ppm/K over the entire temperature range. Thus a SLMS™ or SiC-SLMS™ mirror is comprised of facesheet and foam core materials that have identical CTE. Such CTE uniformity is essential for optical systems that must operate in a cryogenic environment.

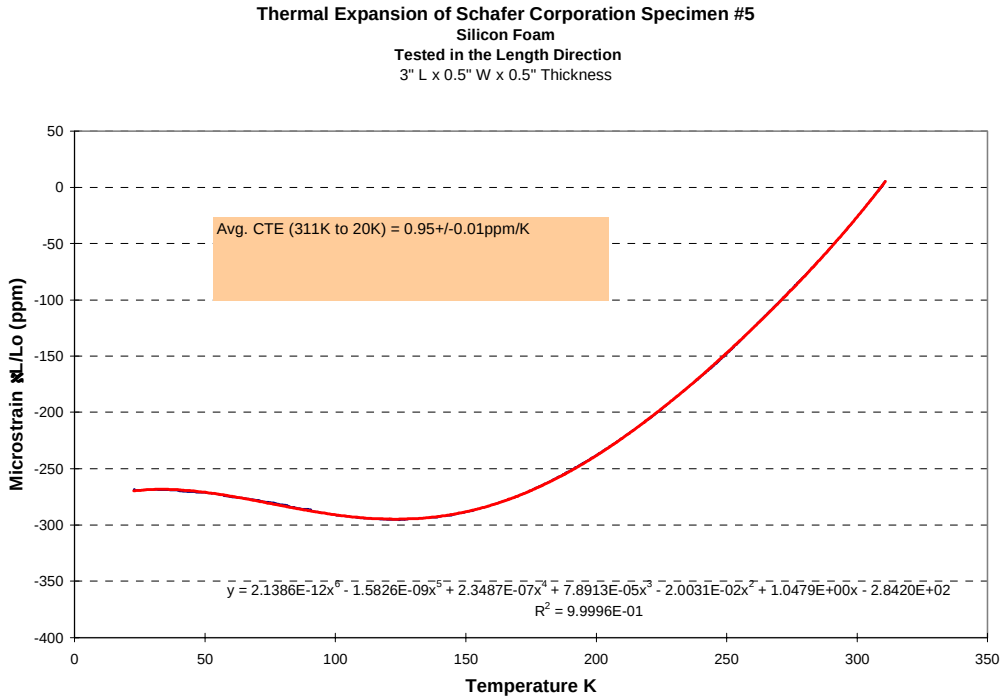

Figure 2. Thermal Strain of Silicon Foam Material (nearly constant below 100 K)

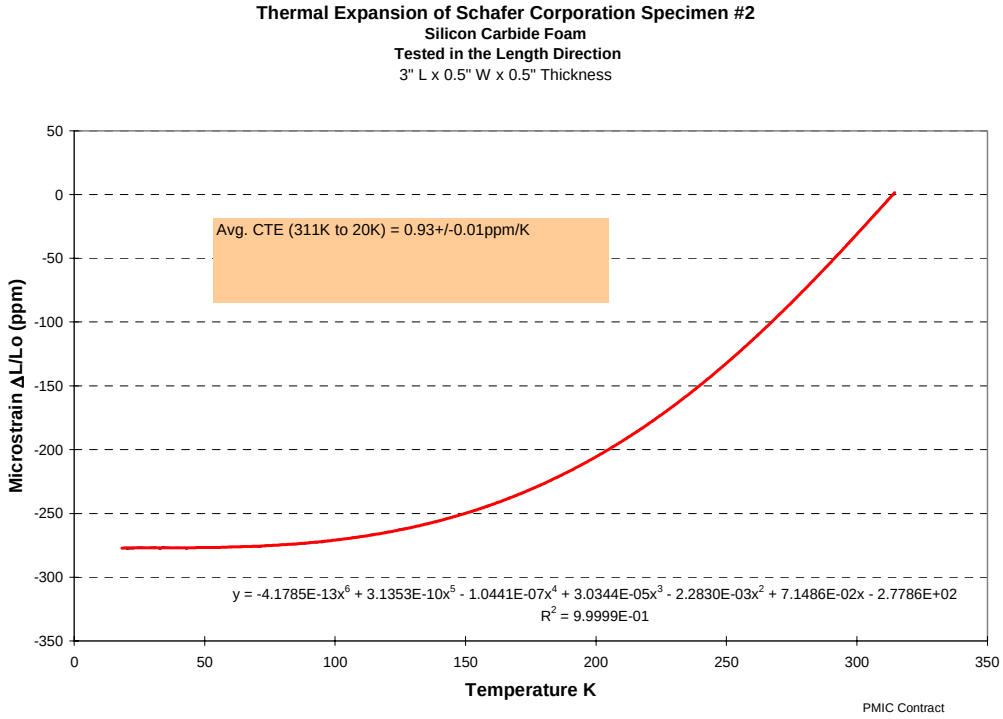

Figure 3. Thermal Strain of Silicon Carbide Foam Material (nearly constant below 100 K)

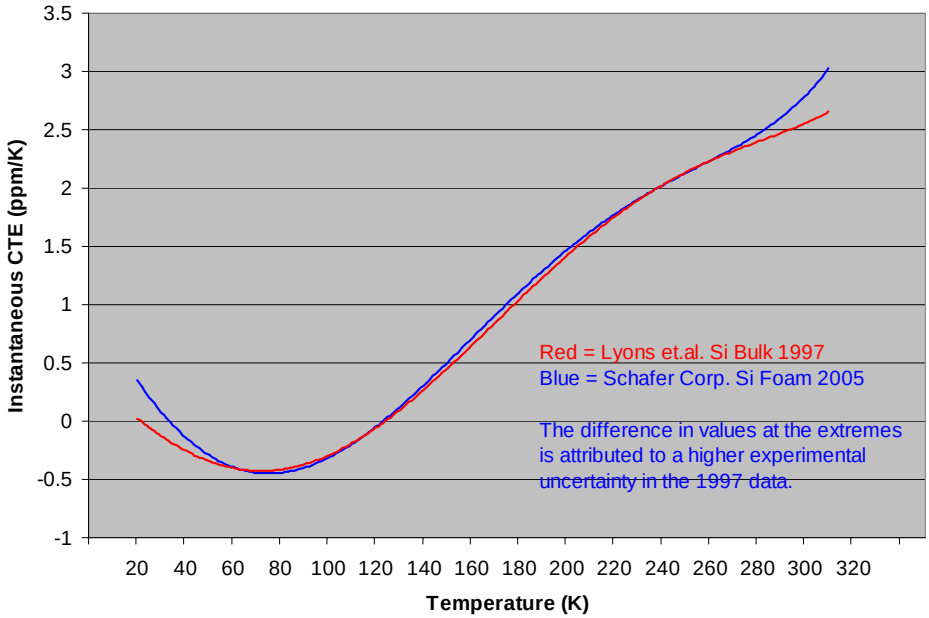

Figure 4. Comparison of Silicon Foam and Bulk CTE

Another major contributing factor to the excellent dimensional stability of SLMS™ and SiC-SLMS™ mirrors is the thermal conductivity of the faceplate and foam core materials. Table 1 provides a comparison of current mirror materials (Zerodure, ULE, Beryllium) with the silicon foam and silicon carbide foam materials at 295 K. The thermal conductivity of the pure silicon or pure beta-silicon carbide skin material is more than 2 orders of magnitude higher than glass or glass-ceramic materials. The table shows that the super-polishable skin of SLMS™ has steady state and transient distortion parameters like the low expansion glasses simultaneously with more than 2 times the specific stiffness (equates to lower mass for the same 1st fundamental frequency of vibration). The table also shows that SiC-SLMS™ has superior thermal performance (transient distortion parameter is 19 times lower) than Beryllium while simultaneously possessing similar structural properties (specific stiffness).

Table 1. Comparison of Material Properties at 295 K

Room Temperature Property:	**Density**	**Young's Modulus**	**Specific Stiffness**	**Tensile Strength**	**Specific Strength**	**Thermal Expansion**	**Thermal Conductivity**	**Specific Heat**	**Thermal Diffusivity**	**Steady State Distortion**	**Transient Distortion**	**Poisson's Ratio**	**Surface Finish**
Units:	kg/m^3	GPa	MPa-m^3/kg	Mpa	MPa-m^3/kg	10^{-6}/K	W/m-K	j/kg-K	10^{-6}/m^2/s	Hm/W	s/m^2-K	arbitrary	nm
Preferred Value:	**Small**	**Large**	**Large**	**Large**	**Large**	**Small**	**Large**	**Large**	**Large**	**Small**	**Small**		**Small**
PRESENT SOTA													
Fused Silica	2190	73	33		0.00	0.5	1.4	750	0.85	0.36	0.59		10
ULE Fused Silica	2210	67	30		0.00	0.015	1.3	770	0.76	0.01	0.02		10
Zerodur	2530	92	36		0.00	-0.09	1.6	810	0.78	-0.06	-0.12		15
Beryllium:I-70 Optical	1850	287	155	237	0.13	11.3	216	1920	60.81	0.05	0.19	0.25	15
SCHAFER TECHNOLOGIES													
Foam Silicon SLMS™ Skin	2330	130	56	120	0.05	2.5	148	750	84.69	0.02	0.03	0.24	5
Foam Beta-SiC SLMS™ Skin	3210	460	143	470	0.15	2.2	380	640	184.97	0.01	0.01	0.21	5
Web Based C/SiC	2655	249	94	150	0.06	2.5	121	800	56.97	0.02	0.04	0.24	10 to 25

The thermal conductivity of the foam material is directly dependent upon the relative density of the ceramic foam as compared to the bulk material. The thermal conductivity of the ceramic foam can range from 3 to 30% of the bulk material, which is from 5-50 W/m-K for silicon foam, and on the order of 10-110 W/m-K for beta-silicon carbide foam.

Thus the thermal conductivity of the ceramic foams can be up to an order of magnitude higher than that of bulk glass or glass-ceramic materials. The sp3 covalent bonding and corresponding lattice structures of the unit cells of silicon and silicon carbide are directly responsible for the simultaneous low CTE and high thermal conductivity of these materials.

As good as the thermal conductivity of silicon is at room temperature, it gets better at deep cryogenic temperatures. Figure 5 compares the CTE and thermal conductivity of solid silicon with beryllium. The thermal conductivity of silicon exceeds 5000 W/m-K at 25 K. A thermal conductivity of 5000 W/m-K at 25 K combined with near-zero CTE means that the static and transient distortion parameters are >30 times lower than Beryllium and >100 times lower than glasses at 25 K. Since the thermal conductivity of the foam material is nominally an order of magnitude lower than the bulk material, then it is seen that silicon foam will have steady state and transient distortion parameters that are >3 times higher than Beryllium and >10 times greater than glasses. As a result, SLMS™ mirrors have been observed to have a figure change of less than $\lambda/100$ rms HeNe from room temperature to 24 K with virtually no print-through of the foam core [3].

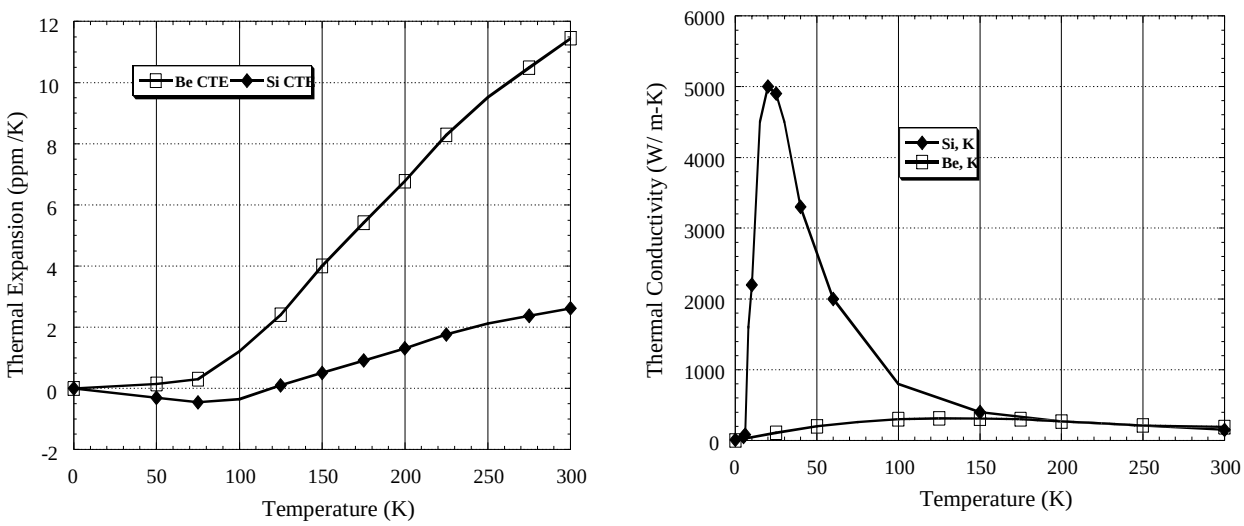

Figure 5. Thermal Properties of Silicon vs. Beryllium at Cryogenic Temperatures

Equally important for cryogenic and laser applications are the mechanical properties of mirror and structure materials. As reported in the literature [4], cryogenic testing of 20-inch long beryllium coupons at Jet Propulsion Laboratory has shown that the damping capability of beryllium decreases with temperature, meaning that the ringdown time following slew will increase for a beryllium mirror as the temperature decreases. Knowing that foams are natural damping materials it was of interest to perform cryogenic damping studies on Schafer's silicon and beta-silicon carbide foam materials. The foremost facility for this type of testing in the world is the Cryogenic Material Damping Testbed at the Jet Propulsion Laboratory, as described in the next section.

3. TEST CONFIGURATION AND SETUP

As illustrated in Figure 6, the Cryogenic Material Damping Testbed at Jet Propulsion Laboratory provided an excellent test facility for all material damping measurements reported in this paper. The tests were performed inside a 0.6 m diameter thermal vacuum chamber equipped with a Gifford-McMahon cycle cryocooler. The system is capable of maintaining the cold finger at any arbitrary temperature between 293 K and 11 K, but for various practical reasons the minimum specimen temperature achieved was 17 K. During the heating or cooling process, the specimen temperature was closely monitored through the Lakeshore 340 Temperature Controller, Figure 7. Pressure inside the chamber was maintained between 10^{-5} to 10^{-6} Pa.

Typical cryogenic damping test specimens of silicon foam and silicon carbide foam, Figure 8, were prismatic rectangular beams with length 508 mm (20 inch), height 50.8 mm (2 inch), and thickness that varied among specimens. An aluminum frame fixture, Figure 6, within the chamber supported each specimen as a pendulum and served as a mounting platform for accessories such as mechanical linkages which control the height of the specimen. Two stainless steel suspension wires of 0.281 mm diameter and 838 mm length were used to suspend the specimen from the aluminum frame fixture. In order to minimize interaction between the specimen bending mode and the modes of the suspension system, the two suspension wires were attached to the top edge of the specimen at the two nodal points of the first transverse free-free bending mode.

The specimen was struck quickly by an impact force. In the initial configuration, a 20 mm diameter solenoid actuator controlled by a switch was used to quickly strike the specimen. For the present tests, a refined technique was employed to enable a repeatable impact force to strike the specimen [4]. This technique replaces the solenoid striker with a curved tube, Figure 6, which guides a 6 mm diameter plastic ball through free-fall to collide with the specimen horizontally. The magnitude of impact force is determined by the mass of the ball.

To shield the specimen from radiation heating, the specimen was enclosed in a copper box-shaped dewar (Figure 6) wrapped in a multi layer insulation blanket. The dewar had small openings for the two specimen suspension wires, for the laser beam to measure the specimen response, and for the curved tube. A temperature sensor (8 mm diameter, 1 gram, brass temperature diode) was attached using an adhesive and capton tape to the specimen just underneath one of the suspension wires. The 0.30 mm sensor lead wire was carefully run up the suspension wire with sufficient slack in the lead to minimize interaction. Additional temperature sensors were used to monitor critical locations within the chamber.

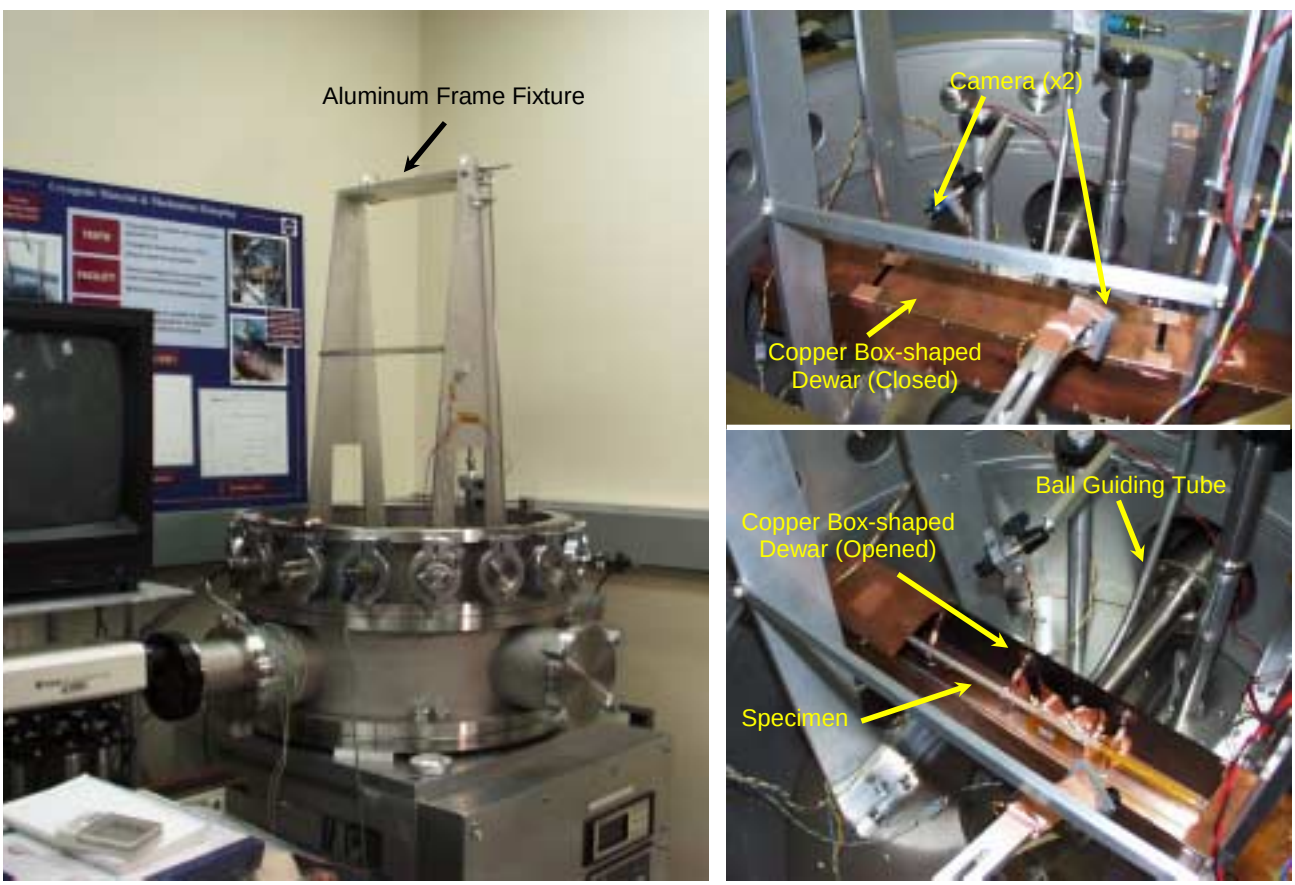

Figure 6. Test Setup of JPL Cryogenic Material Damping Testbed

Figure 7. LakeShore 340 Temperature Controller

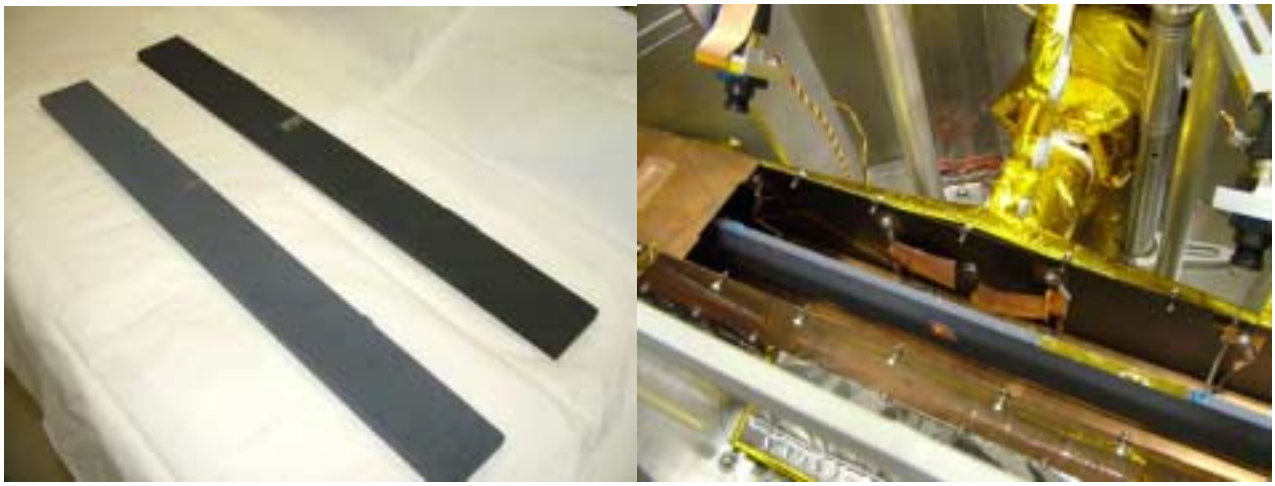

Figure 8. Test Specimens of Silicon Foam and Silicon Carbide Foam

Figure 9. Polytec OFV 3001 Laser Vibrometer

The apparent damping estimates could be increased by at least factor of 2 when a high sensitivity piezoelectric strain gauge and a cryogenic accelerometer were used as witness sensors of the vibrating specimen. The additional damping was induced by the small wires connecting to the sensors [4]. Therefore, these sensors were replaced with a non-contacting laser device, Polytec OFV 3001 Vibrometer to measure transverse velocities of the vibrating specimen, as shown in Figure 9. To enhance the optical diffusivity of the specimens, a 25 mm square piece of retro-reflective tape was attached as a target for the laser beam. Both the impact force and the laser measurements occurred at the geometrical center of the specimen.

Note that a helium tank was attached to the vacuum chamber in later tests in order to control the temperature of the specimen more effectively. The helium was used as a thermal conductor and played a key role in reaching the minimum temperature of 17 K for the composites - the previous limits were around 40 K. To control the temperature of the specimen, the helium gas was released inside the chamber to a pressure level of 10^{-4} to 10^{-5} Pa and then evacuated as the specimen approached the desired temperature.

4. DATA ACQUISITION AND ANALYSIS

The SigLab Data Acquisition System was used to acquire data. This system allows simultaneous monitoring and recording of the data. Acquisition of data started 5 seconds before the specimen was to be excited and continued for 60 seconds total or 55 seconds after the specimen was excited. Absolute velocity of the swinging and vibrating specimen was measured with the laser vibrometer and sampled and digitized with a 16 bit data acquisition system. Depending on the specimen and the expected damping, record lengths of up to 60 seconds at a rate of between 5120 samples/sec and 10240 samples/sec were recorded.

As the specimen was excited by striking with an impact force, the specimen vibration decay, Figure 10, measured by the non-contacting laser vibrometer, was used to determine viscous damping ratios. A digital band-pass filter was applied in the forward and backward directions around the fundamental bending frequency to remove all other modes of vibration and the swinging and twisting pendulum motions.

Measured velocities were then converted to extreme fiber strains using the analytical solution for the fundamental mode shape of a free-free beam, in conjunction with the strain-displacement relationship for Euler-Bernoulli beam theory. The result is dependent only on frequency of vibration and beam thickness (both of which are measured directly), not on material properties. After filtering, the record was searched sequentially and the sample with the maximal positive value in each cycle of vibration was selected and retained, to form an envelope of decaying peak amplitudes.

Working with 250 peak values at a time, a least-squares regression analysis was used to compute the best viscous damping coefficient for that window of data. The 250-sample window was then advanced one peak forward in time and the regression analysis was repeated, continuing until the entire record length had been analyzed and an estimate of viscous damping versus time (or peak amplitude) had been formed. For most records, it was then necessary to average this result across the entire time record because of leakage in the damping estimate at the swinging frequency of the specimen in the pendulum mode.

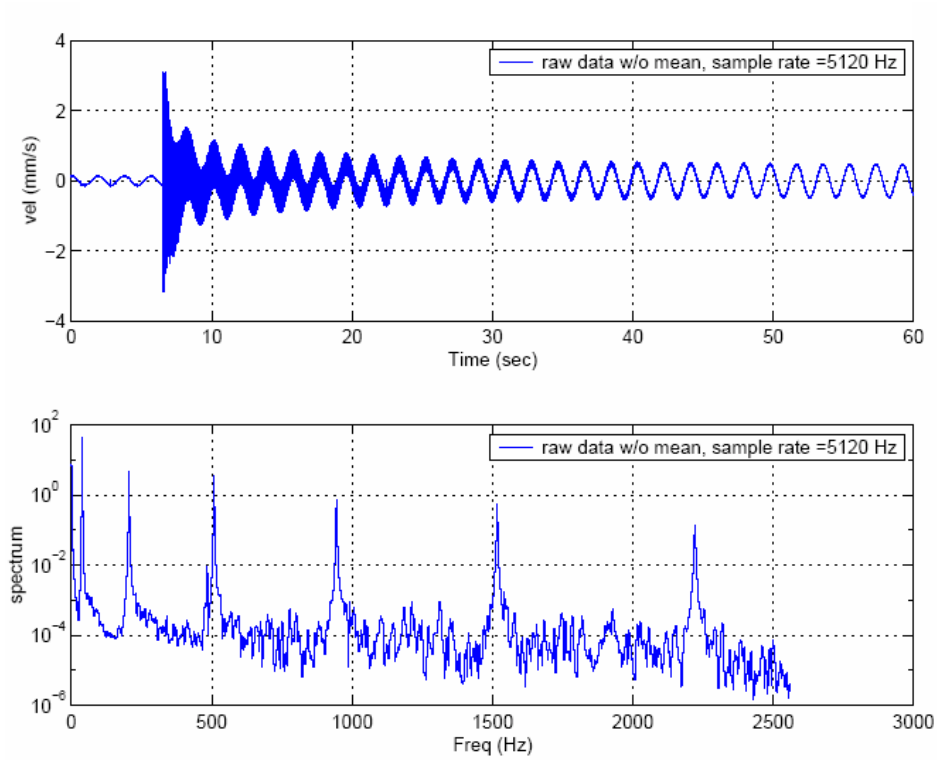

Figure 10. Typical Velocity Measurement of Specimen Vibration Decay

5. THE ZENER DAMPING THEORY

The Zener theory relates damping ξ to temperature, material properties, thickness, and vibration frequency ω as follows:

$$\xi = \frac{\alpha^2 ET}{2C_p\rho}\left[\frac{\omega\tau}{1+(\omega\tau)^2}\right]$$

$$\tau = \frac{C_p h^2 \rho}{\kappa\pi^2}$$

in which α is coefficient of thermal expansion (1/K) , h is specimen thickness (m), E is elastic modulus (N/m^2), T is temperature (K), C_p is specific heat (J/kg/K), κ is thermal conductivity (W/m/K), ρ is density (kg/m^3), ω is frequency of vibration (rad/sec), π is 3.14159, and τ is relaxation time (sec/rad). It is frequently more convenient to work with the relaxation frequency ($1/\tau$) instead.

For b.c.c. and f.c.c. cubic lattice structured metals, Zener theory predicts the thermo-elastic energy loss in beams undergoing cyclic bending strains. Dependence on temperature, frequency, and beam thickness are captured in the theory; however, the theory does not apply for axial and torsional strains, for materials other than b.c.c. and f.c.c metals, or for configurations other than rectangular beams. Many room temperature damping measurements have been made to validate the Zener theory, with much success [5, 6, 7, 8]. Predictive models for material damping in fiber-reinforced composites have been proposed and the available models have been summarized in detail [9].

The thermo-mechanical properties for silicon foam and silicon carbide foam materials are compared with representative thermo-mechanical properties for Aluminum 6061-T6 in Table 2. The foam properties were provided by Schafer Corporation. The aluminum properties were based on handbook values [10, 11]. Note that α, C_p, and κ have a strong dependence on temperature.

During this damping study, samples of same material in various thickness were tested. The measured thickness values of all the six foam samples are listed in Tables 2a & 2b. The purpose is to investigate the change of damping as a function of frequency and correlate the results to the Zener damping theory, which predicts material damping as a function of temperature, modal frequency (or sample thickness), coefficient of thermal expansion and other thermal properties. If we can better understand which of these thermo-mechanical material properties influences the trends of damping at cryogenic temperatures then we can perhaps identify other materials appropriate for very stable cryogenic mechanical systems.

Table 2a. Thermo-Mechanical Properties for Silicon Foam

	CTE (1/K X10^{-6})		E (N/m^2 X10^9)		Cp (J/kg/K)		density (kg/m^3)		k (W/m/K)	
	40K	293K	40K	293K	40K	293K	40K	293K	40K	293K
0.245" thick	-0.15	2.5	4.0	4.0	50	750	342	342	126.3	5.7
0.378" thick	-0.15	2.5	4.0	4.0	50	750	333	333	126.3	5.7
0.500" thick	-0.15	2.5	4.0	4.0	50	750	272	272	103.5	4.6

Table 2b. Thermo-Mechanical Properties for Silicon Carbide Foam

	CTE (1/K X10^{-6})		E (N/m^2 X10^9)		Cp (J/kg/K)		density (kg/m^3)		k (W/m/K)	
	40K	293K	40K	293K	40K	293K	40K	293K	40K	293K
0.245" thick	0	2.2	11.7	11.7	40	640	492	492	44.7	16.2
0.375" thick	0	2.2	11.7	11.7	40	640	509	509	47.5	17.2
0.500" thick	0	2.2	11.7	11.7	40	640	442	442	40.5	14.7

Table 2c. Thermo-Mechanical Properties for Aluminum 6061-T6

	T = 293 K	T = 40 K
α (K^{-1} x10^{-6}) [10]	22.86	15.86
E (N/m^2 x10^9) [10]	68.948	73.602
C_p (J/kg/K) [11]	897	77.5
ρ (kg/m^3) [11]	2713	2713
κ (W/m/K) [11]	158	88.5

6. SUMMARY OF RESULTS

All of the results described herein were measured using 2 inch wide and 20 inch long specimens of various thicknesses. The nominal thickness values of 0.25 inch, 0.375 in and 0.5 inch are used herein to discuss the results. The actual measured thicknesses are listed in Tables 2a & 2b. Testing samples of various thicknesses provides damping values as a function of vibration frequency which is a driving parameter in the Zener damping equation. The tests were conducted in the Cryogenic Material Damping Testbed at the Jet Propulsion Laboratory, as described in Section 3.

Table 3 summarizes the measured damping values and fundamental frequencies at 293 K and 40 K of the silicon foam and silicon carbide foam specimens. The test results are also compared with those of Aluminum 6061-T6 in Table 3. The aluminum data were measured and reported previously in 2004 [12]. The first column in Table 3 shows the thickness of each damping test specimen.

Viscous damping ratios versus temperature are shown in Figures 11a & 11b for the materials of silicon foam and silicon carbide foam, respectively. The damping versus temperature curves of Aluminum 6061-T6 are also plotted in the figures for comparison. Fundamental frequencies versus temperature are shown in Figures 11a and 11b for the materials of silicon foam and silicon carbide foam, respectively.

As compared to Aluminum 6061-T6 in Table 3 and Figures 11a & 11b, both silicon foam and silicon carbide foam materials do not show a significant decrease in damping from room to cryogenic temperatures. The cryogenic damping at 40 K is about 15-20% and 24-68% of the room-temperature damping at 293 K for the samples of silicon foam and silicon carbide foam, respectively. In contrast, the cryogenic damping of aluminum samples at 40 K is decreased significantly to be only 2-7% of their room-temperature damping at 293 K. As observed from the measured damping, the foam specimens have higher damping than aluminum ones at cryogenic temperatures. In addition, the specimens of silicon carbide foam have higher damping than those of silicon foam at cryogenic temperatures.

In contrast to the damping, the fundamental frequencies (or material stiffness properties), as shown in Figures 11a & 11b, are not sensitive to the temperature decreased from room temperatures to cryogenic temperatures. The fundamental frequencies (or material stiffness properties) of both foam materials are almost constant from the room temperature at 293 K to the cryogenic temperature at 40 K, as shown in Table 3.

The damping ratios of silicon foam and silicon carbide foam samples measured at 293 K and 40 K are compared to those predicted by the Zener theory in Table 4. The ratios of the free vibration frequency divided by the Zener relaxation frequency are also computed and tabulated in the table.

Table 3. Damping and Frequencies of Silicon Foam and Silicon Carbide Foam vs. Aluminum at 293 K and 40 K

Silicon Thickness (in)	ζ_{293} **(%)**	ζ_{40} **(%)**	**Ratio** ζ_{40} / ζ_{293}	f_{293} **(Hz)**	f_{40} **(Hz)**	**Ratio** f_{40} / f_{293}
0.25	0.0142	0.0021	0.15	65.330	65.610	1.004
0.375	0.0107	0.0022	0.20	102.62	103.18	1.005
0.5	0.0098	0.0019	0.19	120.00	120.50	1.004
Silicon Carbide Thickness (in)	ζ_{293} **(%)**	ζ_{40} **(%)**	**Ratio** ζ_{40} / ζ_{293}	f_{293} **(Hz)**	f_{40} **(Hz)**	**Ratio** f_{40} / f_{293}
0.25	0.0079	0.0048	0.61	135.41	135.82	1.0030
0.375	0.0099	0.0067	0.68	217.21	217.19	0.9999
0.5	0.0135	0.0032	0.24	269.32	269.24	0.9997
Al 6061-T6 Thickness (in)	ζ_{293} **(%)**	ζ_{40} **(%)**	**Ratio** ζ_{40} / ζ_{293}	f_{293} **(Hz)**	f_{40} **(Hz)**	**Ratio** f_{40} / f_{293}
0.083	0.084	0.0015	0.017	44.44	46.84	1.054
0.125	0.039	0.0017	0.044	63.59	66.99	1.053
0.25	0.0075	0.00055	0.073	125.64	132.38	1.054

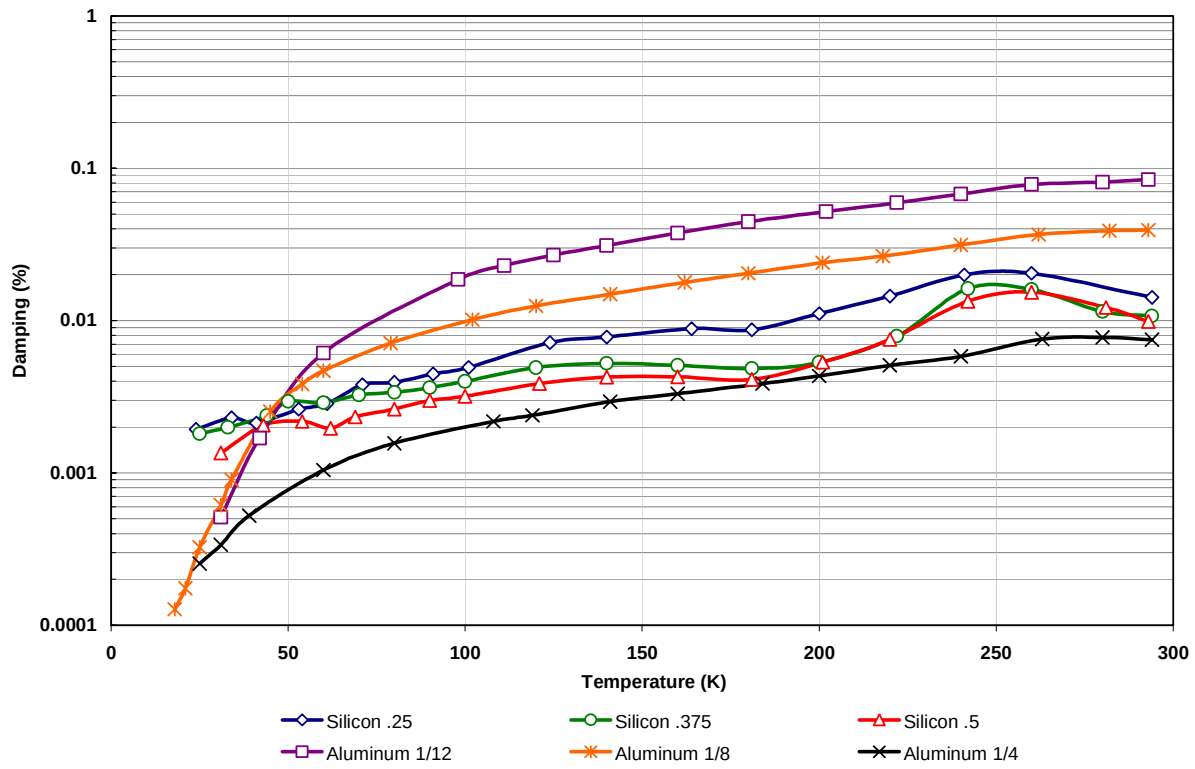

Figure 11a. Damping Ratios vs. Temperatures of Silicon Foam and Aluminum 6061-T6 Samples

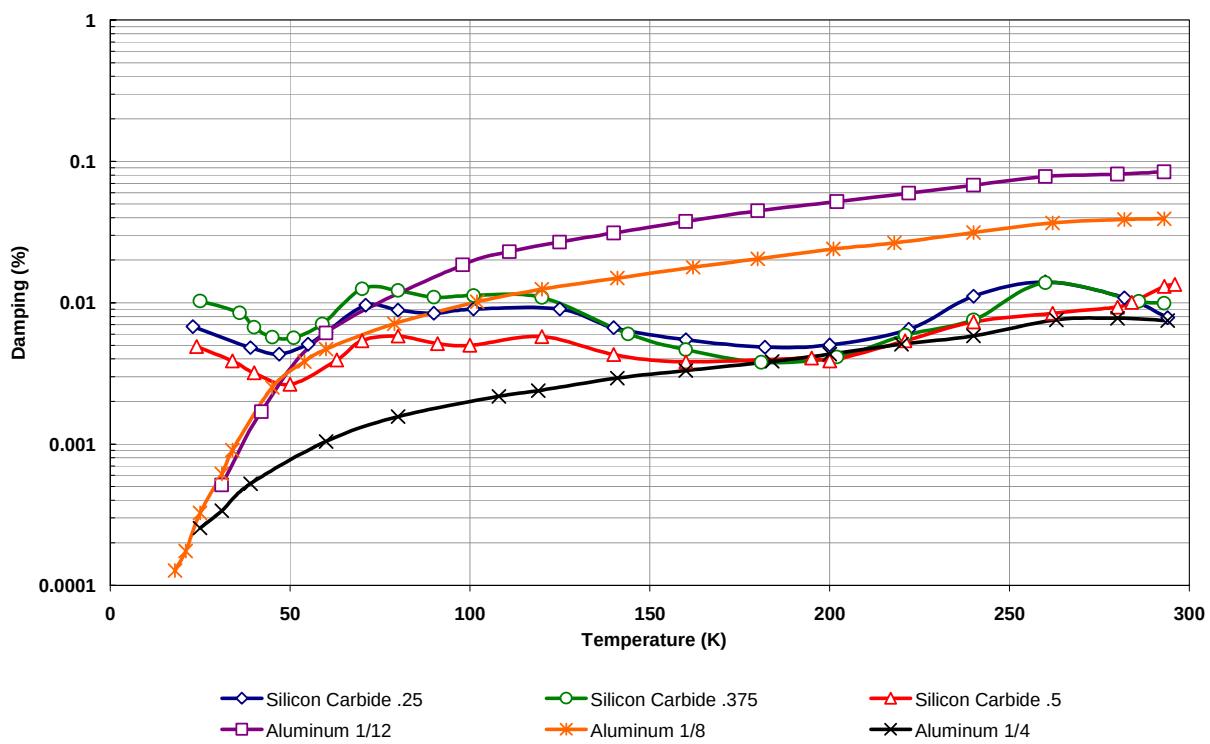

Figure 11b. Damping Ratios vs. Temperatures of Silicon Carbide Foam and Aluminum 6061-T6 Samples

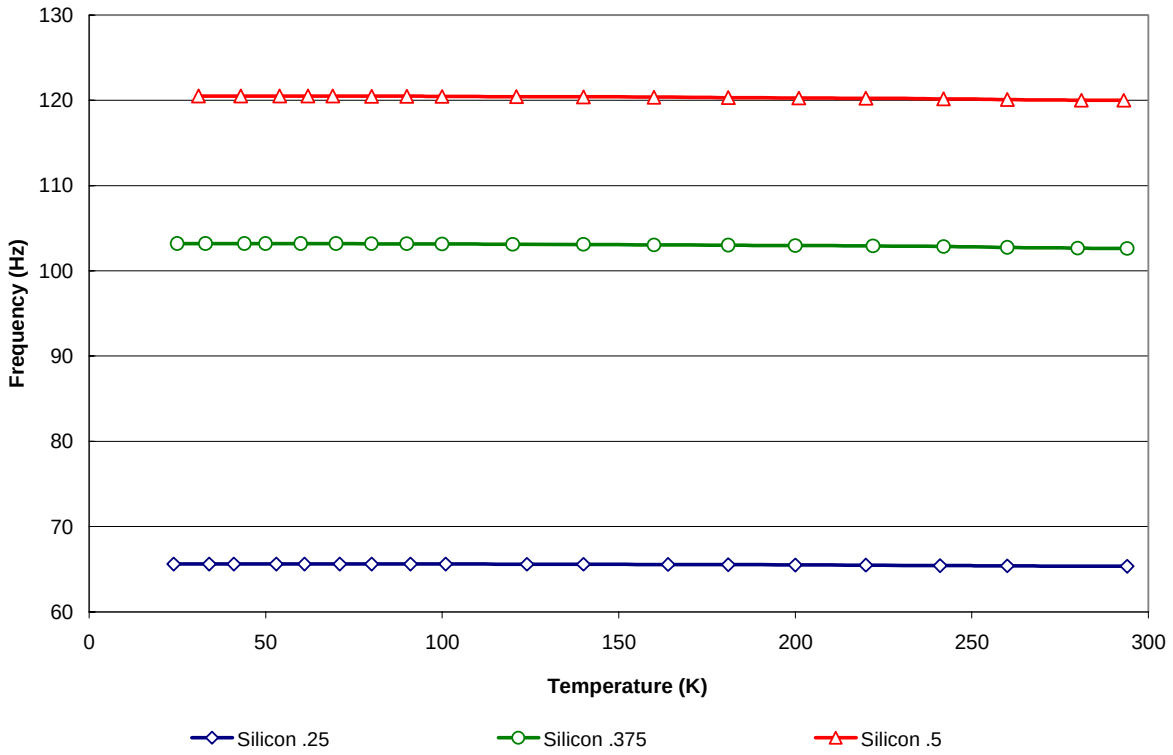

Figure 12a. Frequencies vs. Temperatures of Silicon Foam Samples

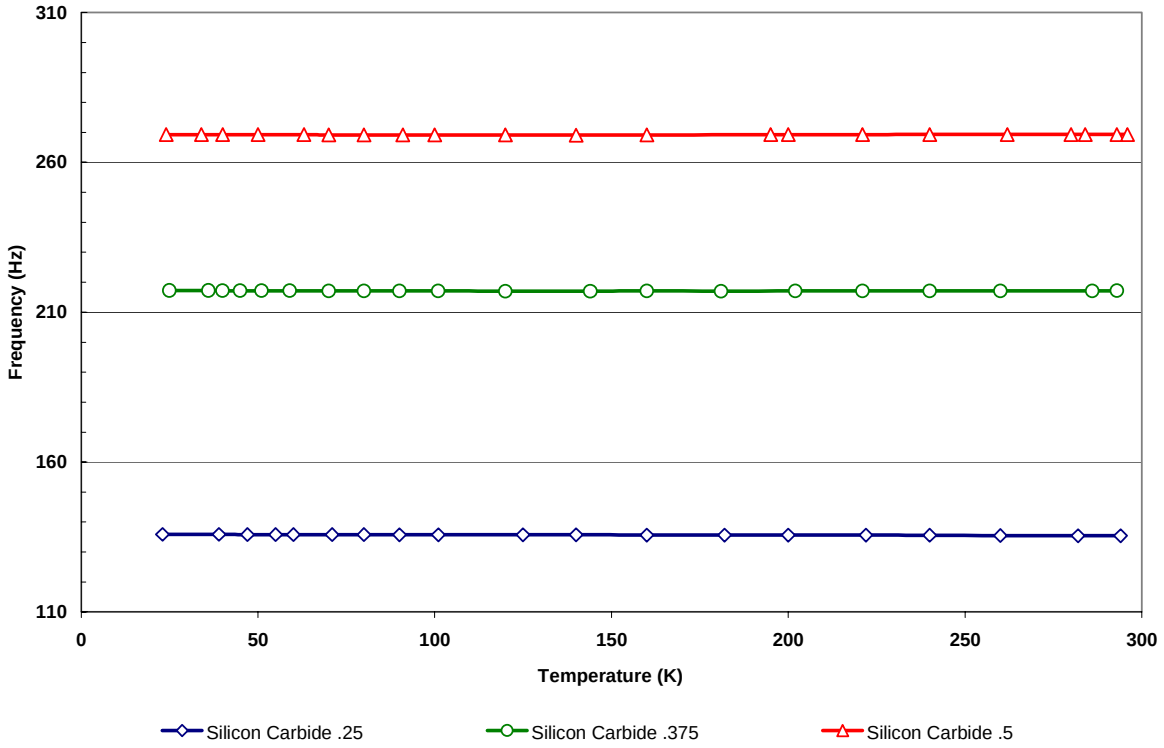

Figure 12b. Frequencies vs. Temperatures of Silicon Carbide Foam Samples

At a room temperature of 293 K, one can observe that the measured damping values and those predicted by the Zener theory do not agree for all the silicon foam and silicon carbide foam samples tested with large frequency ratios. The Zener theory significantly underestimates the damping. This is consistent with the finding reported by previous studies [4, 7, 8, 12]. These studies reveal a trend that the Zener theory underestimates damping at higher frequency ratios, as shown by the aluminum damping data at 293 K in Table 4.

At the cryogenic temperature of 40 K, the damping measurements and the Zener theory do not agree either for all the foam samples tested with large or small frequency ratios. It is apparent that the Zener theory is not applicable to the prediction of damping at cryogenic temperatures for both silicon foam and silicon carbide foam materials. Since the coefficient of thermal expansion is zero at 40 K for the silicon carbide foam, the damping predicted by the Zener theory is zero independent of frequency ratios.

Since the Zener theory cannot predict the damping of silicon foam and silicon carbide foam materials, the damping test is the only reliable way to obtain the material damping at both room and cryogenic temperatures.

Table 4. Damping Comparison vs. Zener Theory for Silicon Foam and Silicon Carbide Foam at 293 K and 40 K

Silicon Thickness (in)	$\zeta_{293,\ measured}$ **(%)**	$\zeta_{293,\ Zener}$ **(%)**	**Ratio** $f_{293,\ measured}$ / $f_{293,\ Zener}$	$\zeta_{40,\ measured}$ **(%)**	$\zeta_{40,\ Zener}$ **(%)**	**Ratio** $f_{40,\ measured}$ / $f_{40,\ Zener}$
0.25	0.0142	1.97e-5	72.5	0.0021	2.20e-6	0.22
0.375	0.0107	5.56e-6	263.9	0.0022	5.27e-6	0.80
0.5	0.0098	3.29e-6	546.4	0.0019	5.91e-6	1.63
Silicon Carbide Thickness (in)	$\zeta_{293,\ measured}$ **(%)**	$\zeta_{293,\ Zener}$ **(%)**	**Ratio** $f_{293,\ measured}$ / $f_{293,\ Zener}$	$\zeta_{40,\ measured}$ **(%)**	$\zeta_{40,\ Zener}$ **(%)**	**Ratio** $f_{40,\ measured}$ / $f_{40,\ Zener}$
0.25	0.0079	4.06e-5	64.9	0.0048	0.0	1.47
0.375	0.0099	1.07e-5	237.6	0.0067	0.0	5.38
0.5	0.0135	5.51e-6	532.2	0.0032	0.0	12.07
Al 6061-T6 Thickness (in)	$\zeta_{293,\ measured}$ **(%)**	$\zeta_{293,\ Zener}$ **(%)**	**Ratio** $f_{293,\ measured}$ / $f_{293,\ Zener}$	$\zeta_{40,\ measured}$ **(%)**	$\zeta_{40,\ Zener}$ **(%)**	**Ratio** $f_{40,\ measured}$ / $f_{40,\ Zener}$
0.083	0.084	0.088	1.95	0.0015	0.051	0.32
0.125	0.039	0.034	6.29	0.0017	0.088	1.02
0.25	0.0075	0.0044	49.7	0.00055	0.022	8.07

6. CONCLUSIONS

Using the test facility of the Cryogenic Material Damping Testbed at the Jet Propulsion Laboratory, an intensive experimental effort has been conducted to provide an insight into the material damping levels at cryogenic temperatures and to search for the materials with high cryogenic damping. The accurate damping test results will enable accurate system level models for prediction and control of instrument disturbances and will enhance the dynamic stability of cryogenic structures for the Terrestrial Planet Finder mission.

Based on the above-described material damping test results of silicon foam and silicon carbide foam materials, these two foam materials have higher damping than aluminum at cryogenic temperatures. It is also observed that their damping levels are relatively insensitive to temperature change from room to cryogenic. As a result, silicon foam and silicon carbide foam materials may be potential candidates to increase levels of cryogenic damping as needed by the Terrestrial Planet Finder mission.

The applicability of the Zener damping theory has been checked for both silicon foam and silicon carbide foam materials. However, large discrepancies are observed between the Zener theory and the test data at both room and cryogenic temperatures. Therefore, the damping test is the only way to estimate the damping levels of these two foam materials at both room and cryogenic temperatures.

Note that these material damping measurements and the observations described above are valid for rectangular beams subjected to bending strains only. Different damping values may be measured as a function not only of material, temperature and frequency, but also of geometry, configuration, strain sense, strain amplitude and environmental effects.

ACKNOWLEDGEMENT

The authors would like to thank the TPF Interferometer project management, Curt Henry and Steve Gunter, for giving their support to the Cryogenic Structures Technology tasks.

The authors would like to thank Lee Peterson and Jason Hinkle from the University of Colorado at Boulder for their technical inputs and discussions.

Extensive technical support by Robert Leland for this task is gratefully acknowledged.

This work was funded jointly by both the TPF Interferometer project and Schafer Corporation. The latter provided its Internal Research and Development funding under a contract with California Institute of Technology.

The experiments were performed at the Jet Propulsion Laboratory, California Institute of Technology, under contract with the National Aeronautics and Space Administration.

REFERENCES

1. G. W. Bush, *"A Renewed Spirit of Discovery: the President's Vision for U.S. Space Exploration,"* U.S. White House Document, January 2004.
2. Curt Henry, Oliver Lay, MiMi Aung, Steven Gunter, Serge Dubovitsky, Gary Blackwood, *"Terrestrial Planet Finder Interferometer: architecture, mission design and technology development,"* SPIE Astronomical Telescopes and Instrumentation, Glasgow, Scotland, June 22, 2004.
3. Marc T. Jacoby, William A. Goodman, H. Philip Stahl, Andrew S. Keys, Jack C. Reily, Ron Eng, James B. Hadaway, William D. Hogue, Jeffrey R. Kegley, Richard D. Siler, Harlan J. Haight, John Tucker, Ernest R. Wright, James R. Carpenter and Jeff E. McCracken, "Helium Cryo Testing of a SLMS^{TM} (Silicon Lightweight Mirrors) Thermal Optical Assembly", Proceedings of SPIE Optical Manufacturing and Testing V, Vol. 5180-26, San Diego, California, August 2003.
4. M. B. Levine and C. V. White, *"Material Damping Experiments at Cryogenic Temperatures,"* Paper No. 5179-25, SPIE Annual Meeting 2005, International Symposium on Optical Science and Technology, San Diego, California, August 2003.
5. Ting, J., E.F. Crawley, *"Characterization of Damping of Materials and Structures at Nanostrain Levels,"* M.S. Thesis, M.I.T., June 1990.
6. Crawley, E.F., G. L. Sarver, and D.G. Moore, *"Experimental Measurement of Passive Material and Structural Damping for Flexible Space Structures,"* Acta Astonautica, Vol. 10, No. 5-6, 1983.
7. Crawley, E.F., M.C. Van Schoor, "*Material Damping in Aluminum and Metal Matrix Composites,"* Journal of Composite Materials, Vol. 21, Jun. 1987.
8. Crawley, E.F., R.L. Sheen, *"Experimental Measurement of Material Damping for Space Structures,"* Proc. Of Vibration Damping Workshop, Long Beach, CA, Feb. 1983.
9. Chandra, R., S. P. Singh, K. Gupta, *"Damping Studies in Fiber-Reinforced Composites – A Review,"* Composite Structures, Vol. 46, 1999.

10. Cryogenic Materials Data Handbook, Air Force Materials Laboratory-Research and Technology Division, Wright-Patterson AFB, July 1965.
11. Cryocomp Computer Program, Version 3.05, Eckels Engineering, Inc., Florence, SC.
12. Chia-Yen Peng, Marie Levine, Lillian Shido and Robert Leland, *"Experimental Observations on Material Damping at Cryogenic Temperatures,"* Paper No. 5528A-7, SPIE Annual Meeting 2004, International Symposium on Space Systems Optomechanics and Dynamics, Denver, Colorado, August 2-6, 2004.